Solutions for the Inclined Borehole in a Porothermoelastic Transversely Isotropic Medium

Younane Abousleiman

Shailesh Ekbote[1]

Mewbourne School of Petroleum and Geological Engineering, School of Civil Engineering and Environmental Science, PoroMechanics Institute, The University of Oklahoma, Norman, OK 73019

A porothermoelastic solution of the general problem of the inclined borehole in a transversely isotropic porous material is presented herein and compared with the isotropic porothermoelastic solution. The governing equations are outlined for the case of general anisotropy and specialized for a transversely isotropic poroelastic material under nonhydrostatic and nonisothermal in situ conditions. A superposition scheme is employed to obtain the analytical solutions within the isotropic and transversely isotropic poromechanics theory. The borehole generator is assumed to coincide with the material axis of symmetry, in the case of transverse isotropy, yet subjected to a three-dimensional state of stress. A systematic analysis has been carried out to evaluate the effect of the anisotropy of the poromechanical material parameters as well as the thermal material properties on stress and pore pressure distributions and the potential impact on the overall stability of deep wellbore drilling. [DOI: 10.1115/1.1825433]

Introduction

A great deal of attention has been focused on coupled thermomechanical behavior of fluid-saturated porous media. Over the years, the theoretical developments in this area have matured from a simple extension of Biot's isotropic poroelastic theory [1–6] to a more general approach which can handle the coupling along with the material anisotropy [7]. Applications for these are found in diverse areas such as deep drilling and excavation, modeling of nuclear waste disposal facilities [8], and extraction of geothermal energy [9]. With the complex mechanisms that come into play, identification of various driving forces and the interaction between them presents a challenge in predicting an appropriate behavior at depth.

Following the work of Biot [1,2], considerable research has been carried out in the mechanics of fluid-saturated porous media. Fundamental aspects of Biot's theory of poroelasticity have been reformulated and presented in various forms [10–12]. Extension of this theory to incorporate thermal effects for the isotropic case has been addressed by several authors [3–6]. Consequently, solutions to boundary and initial value problems have been developed under various scenarios which demonstrate the effect of the thermohydromechanical coupling on the response [13–18].

At the same time, Biot's theory has been extended to account for material anisotropy [2,11]. The extension introduced various material constants which were identified and recast with straightforward physical interpretations [19,20]. Subsequently, analytical solutions for fundamental problems such as Mandel's problem [21], the borehole problem, and the cylinder problem [22] have been extended for the transversely isotropic case. It was found that analysis of the transversely isotropic poroelastic problems showed unpredicted results when compared to their elastic counterparts [21,22]. In addition to the time dependency of the flow and deformation fields, the anisotropic material coefficients play an important role in the calculation of the in-plane stresses. There is existing literature that addresses the thermal effects in anisotropic media, though the treatment in many cases is limited to coupled thermoelasticity [23–25]. A comprehensive treatment of the anisotropic porothermoelasticity has been addressed by Katsube [7].

In general, geoactivities are usually carried out in formations that can be broadly classified as transversely isotropic due to the simple natural deposition of sedimentary rocks which has occurred over a geological time scale. The deposition processes lead to development of formations with similar material properties across a cross section but with different characteristics in the direction perpendicular to it. In this paper, a porothermoelastic solution for an inclined borehole in a transversely isotropic medium is presented. Governing equations are developed first for general anisotropy and then specialized for the transversely isotropic and isotropic cases. The resulting system of equations is used to obtain the analytical solution for an infinitely long borehole where it is assumed that the borehole generator coincides with the material axis of symmetry.

General Formulations

Upon load application, the mechanical response of a fluid-saturated porous system is characterized by coupled diffusion–deformation attributed to the interdependence of change in pore volume and the pore fluid pressure. With the introduction of boundary temperatures, i.e., a nonisothermal state, both the pore fluid and pore volume are subject to differential expansion or contraction, resulting in additional coupling associated with the temperature change. The magnitude of the relative change in stress, pore pressure, and temperature is coupled and described by constitutive relations weighted by material coefficients. In this section, a full set of governing equations is developed for the general anisotropic case.

Constitutive Equations. The constitutive equations for linear porothermoelasticity are expressed as [5,6]

$$\sigma_{ij} = M_{ijkl}\epsilon_{kl} - \alpha_{ij}p - \beta^{s}_{ij}T \tag{1a}$$

$$\zeta = p/M + \alpha_{ij}\epsilon_{ij} - \beta^{sf}T \tag{1b}$$

Equations (1*a*) and (1*b*) are written using a tension positive convention. The above equations relate the response of the dynamic variables, σ_{ij} (total stress tensor), p (pore pressure), and T (temperature), to the kinematic quantities, ϵ_{ij} (solid strain tensor) and ζ (variation of fluid content). The connection between the dy-

[1]Now at Shell International Exploration and Production, Houston, TX 77025.

Contributed by the Applied Mechanics Division of THE AMERICAN SOCIETY OF MECHANICAL ENGINEERS for publication in the ASME JOURNAL OF APPLIED MECHANICS. Manuscript received by the Applied Mechanics Division, January 21, 2004; final revision, March 18, 2004. Editor: R. M. McMeeking. Discussion on the paper should be addressed to the Editor, Prof. Robert M. McMeeking, Journal of Applied Mechanics, Department of Mechanical and Environmental Engineering, University of California—Santa Barbara, Santa Barbara, CA 93106-5070, and will be accepted until four months after final publication in the paper itself in the ASME JOURNAL OF APPLIED MECHANICS.

namic and kinematic quantities is characterized by the material constants, M_{ijkl} (drained elastic modulus tensor), α_{ij} (Biot's effective stress coefficient tensor), M (Biot's modulus), β^s_{ij} (thermic coefficient tensor related to the solid skeleton), and β^{sf} (thermic coefficient related to the pore fluid). The thermic coefficient tensor, β^s_{ij}, provides a measure of the stress induced due to change in temperature. It is related to the thermal expansion coefficients and the drained elastic modulus tensors as follows [26,27]:

$$\beta^s_{ij} = M_{ijkl}\alpha^s_{kl} \tag{2}$$

where α^s_{ij} is the linear expansion coefficient tensor of the solid skeleton. The thermic coefficient, β^{sf}, on the other hand, is associated with the pore fluid and provides a measure of the pore pressure induced due to a change in temperature. It is related to the thermal expansion coefficients of the solid–fluid system, the porosity to the medium, and the Biot's effective stress coefficient tensor, and is given as [28,29]

$$\beta^{sf} = \alpha_{ij}\alpha^s_{ij} + (\alpha^f - \alpha^s_{kk})\phi \tag{3}$$

in which α^f is the volumetric expansion coefficient for the pore fluid, and ϕ is the porosity. Note that in writing Eqs. (1)–(3), the thermal expansion coefficients of the bulk drained material and that of the solid skeleton are assumed to be equal. The above equations give the complete anisotropic stress–strain response of a porothermoelastic material. For the most general anisotropic case, the behavior is described using 35 constants (21 M_{ijkl}'s, 6 α_{ij}'s, 1 M, 6 β^s_{ij}'s, and 1 β^{sf}) [30].

Mass Balance. Under isothermal coditions, Darcy's law, where the fluid flux is proposional to the pressure gradient, is well known [6]. For solid–fluid constituent porous system, where no fluid sources or sinks exist, the fluid mass balance equation is written as

$$\frac{\partial \zeta}{\partial t} + q_{i,i} = 0 \tag{4}$$

where q is the specific discharge vector. Under nonisothermal conditions fluid transport within the system can be caused by a gradient in both the pore fluid pressure as well as temperature. A generalized expression for the specific discharge, q, is given as [15]

$$q_i = -\kappa_{ij}p_{,j} + \Gamma^q_{ij}T_{,j} \tag{5}$$

in which κ_{ij} is the anisotropic mobility coefficient tensor and Γ^q_{ij} is the coefficient tensor which relates the flux to the temperature gradient. The first term on the right-hand side in Eq. (5) corresponds to the fluid transport caused by the *Darcy* effect and the second term on the right-hand side corresponds to the fluid flux generated as a result of the *Soret* effect. The term associated with the *Soret* effect is ignored in this analysis, and Eq. (5) results in the well-known Darcy's law. The anisotropic mobility coefficient tensor, κ_{ij}, is related to the intrinsic permeability tensor, k_{ij}, and the pore fluid viscosity, μ, by $\kappa_{ij} = k_{ij}/\mu$.

Momentum Balance. Momentum balance yields the equilibrium equations which are given by

$$\sigma_{ij,j} = 0 \tag{6}$$

Again, Eq. (6) has been written, in terms of the total stress approach, while ignoring any body and inertial forces.

Energy Balance. Within a continuum model, both the matrix and the pore fluid are assumed to occupy the same point in space and therefore one should introduce two temperatures to characterize the thermal state of the system. However, existing studies for thermomechanical behavior of porous media employ a common temperature for both the constituents of the porous system based on the assumption of instantaneous local temperature equilibrium [3,4,15,16,31]. In other words, it is assumed that the heat transport between the matrix and the pore fluid at the local level is much faster than the overall heat diffusion process. Neglecting the internal energy change due to viscous dissipation and compression, the energy balance equation is given as

$$\rho C_v \frac{\partial T}{\partial t} = -h_{i,i} - (\rho C_v q_i)T_{,i} \tag{7}$$

where ρC_v is the heat capacity of the solid–fluid mixture and h is the heat flux. In Eq. (7) the first term on the right-hand side corresponds to heat transport by conduction, whereas the second term represents the heat transport by convection. In addition, it is assumed that the porous material bears a low permeability and that the heat diffusion occurs much faster than the fluid diffusion, which indirectly results in the assumption of a small *Peclet* number. Under these circumstances, the term corresponding to convection can be dropped from (7), resulting in a linearized form of the energy balance given by

$$\rho C_v \frac{\partial T}{\partial t} + h_{i,i} = 0 \tag{8}$$

Clearly, Eq. (8) is uncoupled from the pore pressure field.

The "bulk heat capacity," ρC_v, can be related to individual heat capacities of the solid and fluid constituents by [3,15]

$$\rho C_v = (1-\phi)\rho^s C^s_v + \phi\rho^f C^f_v \tag{9}$$

in which the superscripts s and f refer to the solid and fluid, respectively.

Analogous to the fluid mass transport, the heat flux in the most general case can be caused by gradients in pressure and temperature. A generalized equation for the heat flux is given by [15]

$$h_i = -\lambda_{ij}T_{,j} + \Gamma^h_{ij}p_{,j} \tag{10}$$

where λ_{ij} is the effective thermal conductivity of the solid–fluid system, and Γ^h_{ij} is the coefficient tensor associated with the heat flux caused by the pressure gradient. The first term on the right-hand side in Eq. (10) is the heat flux caused by the *Fourier* effect, whereas the second term gives the heat flux resulting from the *Dufour* effect. The *Dufour* effect is ignored in this analysis, thus giving the governing equation for the heat flux also known as Fourier's law.

As in Eq. (9) the "effective thermal conductivity" can also be obtained from the thermal conductivities of the solid and fluid constituents as a weighted average using the porosity, and is given as [3,15]

$$\lambda_{ij} = (1-\phi)\lambda^s_{ij} + \phi\lambda^f_{ij} \tag{11}$$

where λ^s_{ij} and λ^f_{ij} are the thermal conductivities of the solid and fluid constituents, respectively.

The above set of Eqs. (1)–(11) represents the porothermoelastic system in the general anisotropic form. These are specialized for a transversely isotropic material in the next section.

Transversely Isotropic Material

A transversely isotropic material is characterized by same properties in one plane and different properties in the direction normal to this plane. For the transversely isotropic material it is assumed that the z axis coincides with the axis of elastic symmetry. The transversely isotropic poroelastic material is characterized by 8 material constants [19,20]. These are given as E, E', ν, ν', G', α, α', and M, where the unprimed variables are material coefficients in the isotropic plane and the primed variables are material coefficients in the transverse direction. In the above, E is the drained elastic modulus, ν is the drained Poisson's ratio, G is the shear modulus, α is the Biot's effective stress coefficient, and M is the

Biot's modulus. With the introduction of nonisothermal effects three additional thermic constants, β^s, $\beta^{s'}$, β^{sf} are required to account for the differential volume change of the solid skeleton and pore fluid due to temperature changes. Hence, constitutive relations for the transversely isotropic material under nonisothermal conditions are given as follows:

$$\begin{Bmatrix} \sigma_{xx} \\ \sigma_{yy} \\ \sigma_{zz} \\ \tau_{xy} \\ \tau_{yz} \\ \tau_{zx} \\ p \end{Bmatrix} = \begin{bmatrix} \bar{M}_{11} & \bar{M}_{12} & \bar{M}_{13} & 0 & 0 & 0 & -\alpha M \\ \bar{M}_{12} & \bar{M}_{11} & \bar{M}_{13} & 0 & 0 & 0 & -\alpha M \\ \bar{M}_{13} & \bar{M}_{13} & \bar{M}_{33} & 0 & 0 & 0 & -\alpha' M \\ 0 & 0 & 0 & G & 0 & 0 & 0 \\ 0 & 0 & 0 & 0 & G' & 0 & 0 \\ 0 & 0 & 0 & 0 & 0 & G' & 0 \\ -\alpha M & -\alpha M & -\alpha' M & 0 & 0 & 0 & M \end{bmatrix} \begin{Bmatrix} \epsilon_{xx} \\ \epsilon_{yy} \\ \epsilon_{zz} \\ \gamma_{xy} \\ \gamma_{yz} \\ \gamma_{zx} \\ \zeta \end{Bmatrix} - \begin{bmatrix} \bar{\beta}^s \\ \bar{\beta}^s \\ \bar{\beta}^{s'} \\ 0 \\ 0 \\ 0 \\ M\beta^{sf} \end{bmatrix} T \tag{12}$$

where

$$\bar{M}_{11} = M_{11} + \alpha^2 M; \quad \bar{M}_{12} = M_{12} + \alpha^2 M \tag{13a}$$

$$\bar{M}_{13} = M_{13} + \alpha\alpha' M; \quad \bar{M}_{33} = M_{33} + \alpha'^2 M \tag{13b}$$

$$\bar{\beta}^s = \beta^s + \alpha M \beta^{sf}; \quad \bar{\beta}^{s'} = \beta^{s'} + \alpha' M \beta^{sf} \tag{13c}$$

In the above, the coefficients of the drained elastic modulus tensor can be related to the material constants E, E', ν, ν', and G' chosen to represent the transversely isotropic materials by the following relations [20–22]:

$$M_{11} = \frac{E(E' - E\nu'^2)}{(1+\nu)(E' - E'\nu - 2E\nu'^2)};$$

$$M_{12} = \frac{E(E'\nu + E\nu'^2)}{(1+\nu)(E' - E'\nu - 2E\nu'^2)} \tag{14a}$$

$$M_{13} = \frac{EE'\nu'}{(E' - E'\nu - 2E\nu'^2)}; \quad M_{33} = \frac{E'^2(1-\nu)}{(E' - E'\nu - 2E\nu'^2)} \tag{14b}$$

In addition, it has been shown that, with the assumption of microisotropy and microhomogeneity the coefficients α and α' can be related to components of the drained elastic tensor [19,20]. These relations are given as

$$\alpha = 1 - \frac{M_{11} + M_{12} + M_{13}}{3K_s} \tag{15a}$$

$$\alpha' = 1 - \frac{2M_{13} + M_{33}}{3K_s} \tag{15b}$$

where K_s is the grain bulk modulus of the solid constituent. Similarly, using Eqs. (2) and (3), expressions for β^s, $\beta^{s'}$, and β^{sf} are obtained as follows:

$$\beta^s = (M_{11} + M_{12})\alpha^s + M_{13}\alpha^{s'} \tag{16a}$$

$$\beta^{s'} = 2M_{13}\alpha^s + M_{33}\alpha^{s'} \tag{16b}$$

$$\beta^{sf} = 2\alpha\alpha^s + \alpha'\alpha^{s'} + (\alpha^f - 2\alpha^s - \alpha^{s'})\phi \tag{16c}$$

where α^s and $\alpha^{s'}$ are coefficients of linear expansion of the solid skeleton in the isotropic plane and transverse directions, respectively. In addition, the transversely isotropic material is characterized by different thermal conductivities (λ,λ') and mobility coefficients (κ,κ') in the isotropic plane and transverse directions. In line with the aforementioned discussion, governing equations for a three-dimensional case can be derived.

However, many problems in geomechanics are characterized by geometries in which boundary conditions do not change along the direction of their generators. Under such circumstances, a generalized plane strain idealization can be used which allows extrapolation of solutions developed in two-dimensional geometries to a general three-dimensional case [32,33].

It is assumed that the z direction is infinitely long and that boundary conditions are invariant along that direction. Hence, a generalized plane strain condition, as discussed above, manifests itself, resulting in all stress components, pore pressure, and temperature being z independent. Naturally, both heat and fluid flux components in the z direction vanish and all diffusion phenomena occur in the $x-y$ plane which is isotropic. It would therefore be useful to derive governing equations for a plane $(x-y)$ case which will be utilized in obtaining analytical solutions (two-dimensional) and subsequently extended to the three-dimensional case under the assumption of a generalized plane strain condition.

Combination of the equilibrium equations with the constitutive relations yields the Navier-type equations which are given as follows:

$$\tfrac{1}{2}(M_{11} - M_{12})u_{i,jj} + \tfrac{1}{2}(M_{11} + M_{12})u_{j,ji} = \alpha p_{,i} + \beta^s T_{,i} \quad (i,j = 1,2) \tag{17}$$

where u_i denotes the solid displacement. Note that the two-dimensional form of the equilibrium equations has been used to derive the above equation.

Combining the energy balance relation with Fourier's law yields the heat diffusion equation

$$\frac{\partial T}{\partial t} - c_h \nabla^2 T = 0 \tag{18}$$

where $c_h = \lambda/\rho C_v$ is the heat diffusivity in the isotropic plane.

Diffusion equations for the pore fluid are obtained combining the fluid mass balance relations with Darcy's law. These can be expressed in terms of the pore pressure, p, and the variation of the fluid content ζ, and are given as

$$\frac{\partial p}{\partial t} - \kappa M \nabla^2 p = -\alpha M \frac{\partial \epsilon}{\partial t} + \beta^{sf} M \frac{\partial T}{\partial t} \tag{19a}$$

$$\frac{\partial \zeta}{\partial t} - c_f[\nabla^2 \zeta + \bar{c}\nabla^2 T] = 0 \tag{19b}$$

where $\epsilon = \epsilon_{xx} + \epsilon_{yy}$ and $\bar{c}$ are, respectively, the fluid diffusivity and a coupling constant in accordance with

$$c_f = \frac{\kappa M M_{11}}{(M_{11} + \alpha^2 M)} \tag{20a}$$

$$\overline{c}=\frac{\alpha\beta^s-M_{11}\beta^{sf}}{M_{11}} \tag{20b}$$

In addition, the pore pressure diffusion equation [Eq. 19(*a*)] can be simplified assuming an irrotational displacement field and a semi-infinite domain, and is expressed as

$$\frac{\partial p}{\partial t}-c_f\nabla^2 p=c_{hf}\frac{\partial T}{\partial t} \tag{21}$$

where c_{hf} is a coupling constant given by

$$c_{hf}=\frac{c_f}{\kappa}\left(\beta^{sf}-\frac{\alpha\beta^s}{M_{11}}\right) \tag{22}$$

Notice that although governing equations are written here in their two-dimensional forms [Eqs. (17)–(22)], their coefficients are still dependent on the material elastic properties in the transverse direction. However, since the heat and fluid flux in the z direction vanish under a generalized plane strain idealization, the respective conductivities (κ' and λ') are redundant.

The Navier-type equations (17), heat diffusion equation (18), and the pore pressure diffusion equation in an irrotational displacement field, Eq. (21), constitute a set of complete equations which can be solved to obtain solutions at the stress level. Clearly, the heat diffusion equation is uncoupled from the fluid diffusion and deformation fields and can be solved independently to yield expressions for the temperature distribution. These expressions for the temperature field are then used in the pore pressure diffusion equation [Eq. (21)] to obtain expressions for the pore pressure which can in turn be used within the Navier-type equations [Eq. (17)] to obtain solutions for the stress field.

Isotropic Material

Under the special case where the material is isotropic, the material is identified by two elastic constants, G and ν, two poroelastic constants, α and M, and two thermic coefficients, β^s and β^{sf}. It can be shown that the constitutive equations reduce to

$$\sigma_{ij}=2G\epsilon_{ij}+\frac{2G\nu}{1-2\nu}\epsilon\delta_{ij}-\alpha p\,\delta_{ij}-\beta^s T\delta_{ij} \tag{23a}$$

$$p=M(\zeta-\alpha\epsilon+\beta^{sf}T) \tag{23b}$$

$$\beta^s=\frac{2G(1+\nu)}{(1-2\nu)}\alpha^s \tag{23c}$$

$$\beta^{sf}=3\alpha\alpha^s+(\alpha^f-3\alpha^s)\phi \tag{23d}$$

The other governing equations are given as

Heat Diffusion

$$\frac{\partial T}{\partial t}-c_h\nabla^2 T=0 \tag{24}$$

Fluid Diffusion

$$\frac{\partial p}{\partial t}-\kappa M\nabla^2 p=-\alpha M\frac{\partial\epsilon}{\partial t}+\beta^{sf}M\frac{\partial T}{\partial t} \tag{25a}$$

$$\frac{\partial\zeta}{\partial t}-c_f[\nabla^2\zeta+\overline{c}\nabla^2 T]=0 \tag{25b}$$

Under the assumptions of an irrotational displacement field and semi-infinite domain, the pore pressure diffusion equation [Eq. 25(*a*)] reduces to

$$\frac{\partial p}{\partial t}-c_f\nabla^2 p=c_{hf}\frac{\partial T}{\partial t} \tag{26}$$

Navier Equations

$$Gu_{i,jj}+\frac{G\nu}{1-2\nu}u_{j,ji}=\alpha p_{,i}+\beta^s T_{,i} \tag{27}$$

and c_f, c_{hf}, and $\overline{c}$ reduce to their isotropic counterparts and are given by

$$c_f=\frac{2G\kappa(1-\nu)(\nu_u-\nu)}{\alpha^2(1-2\nu)^2(1-\nu_u)} \tag{28a}$$

$$c_{hf}=\frac{c_f}{\kappa}\left(\beta^{sf}-\alpha\alpha^s\frac{(1+\nu)}{(1-\nu)}\right) \tag{28b}$$

$$\overline{c}=\left(\alpha\alpha^s\frac{(1+\nu)}{(1-\nu)}-\beta^{sf}\right) \tag{28c}$$

Inclined Borehole Problem

It is assumed that an infinitely long borehole is drilled perpendicular to the isotropic plane of a transversely isotropic poroelastic formation. The borehole is inclined and its axis deviated from the in situ stress orientation. A schematic of the inclined borehole is shown in Fig. 1(*a*). The formation, described using a Cartesian coordinate system $x'y'z'$, is characterized by in situ stresses $S_{x'}$, $S_{y'}$, and $S_{z'}$, virgin pore pressure p_0, and formation temperature T_0. The borehole deviation is measured by two angles φ_z and φ_y, which are the inclination and azimuth angles, respectively. A local coordinate system is chosen to represent the borehole in which the z axis is assumed to coincide with the borehole axis. The far-field in situ stresses in the $x'y'z'$ coordinate system are transformed to the local xyz coordinate system via a transformation matrix [32]. In the local coordinate system, the borehole is subject to normal as well as shear components of stress given as S_x, S_y, S_z, S_{xy}, S_{xz}, and S_{yz}, as shown in Fig. 1(*b*).

The boundary conditions of the problem can be imposed at the far field, $r\to\infty$

$$\sigma_{xx}=-S_x;\quad \sigma_{yy}=-S_y;\quad \sigma_{zz}=-S_z; \tag{29a}$$

$$\tau_{xy}=-S_{xy};\quad \tau_{yz}=-S_{yz};\quad \tau_{xz}=-S_{xz}; \tag{29b}$$

$$p=p_0;\quad T=T_0 \tag{29c}$$

and at the borehole wall, $r=R$

$$\sigma_{rr}=-p_w H(t);\quad \tau_{r\theta}=\tau_{rz}=0; \tag{30a}$$

$$p=p_w H(t);\quad T=T_w H(t) \tag{30b}$$

where p_w is the wellbore pressure, T_w is the wellbore fluid temperature, and $H(t)$ is the Heaviside unit step function.

Owing to linearity of the problem, the solution is obtained employing a superposition of three subproblems [32]. Of these, the first problem is a modified plane strain problem which accounts for the in-plane normal and shear stresses and the pore pressure and temperature perturbations. This problem shows full coupling of the fluid and heat diffusion processes with the deformation. The other two problems, which are described as the uniaxial problem and the anti-plane problem [33], are purely elastic since they do not trigger fluid or heat diffusion.

The boundary conditions in the decomposition scheme are given as follows:

Problem 1:

At far field ($r\to\infty$)

$$\sigma_{xx}=-S_x;\quad \sigma_{yy}=-S_y;\quad \tau_{xy}=-S_{xy} \tag{31a}$$

$$\sigma_{zz}=-\nu'(S_x+S_y)-(\alpha'-2\nu'\alpha)p_0-(\beta^{s'}-2\nu'\beta^s)T_0 \tag{31b}$$

$$\tau_{yz}=\tau_{xz}=0 \tag{31c}$$

$$p=p_0;\quad T=T_0 \tag{31d}$$

At the borehole wall ($r=R$)

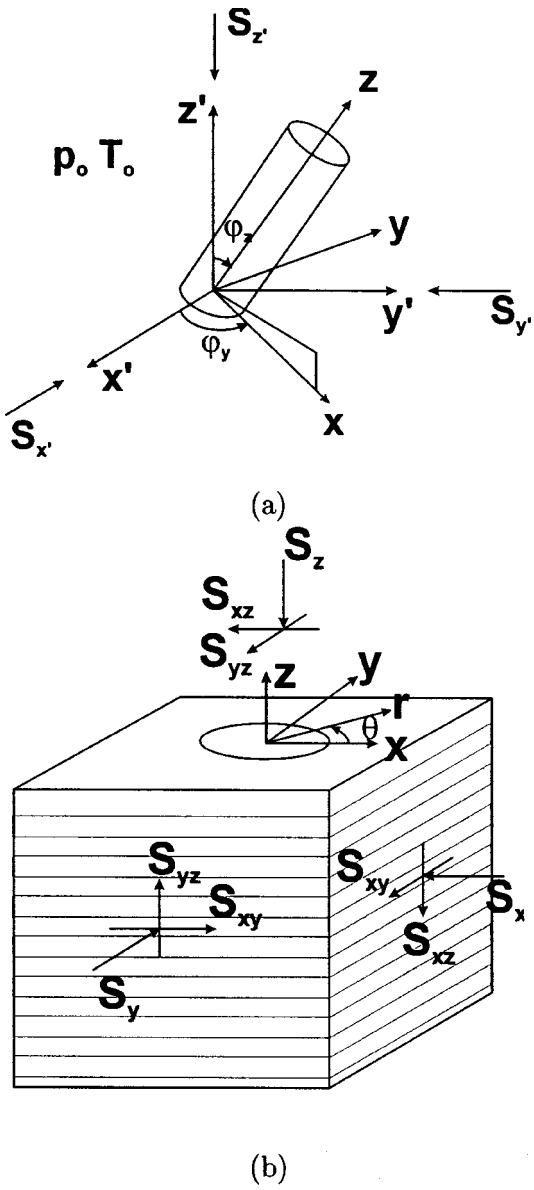

Fig. 1 (*a*) Schematic of an inclined borehole; (*b*) Far-field stresses in the *xyz* coordinate system

$$\sigma_{rr}=-p_w H(t); \quad p=p_w H(t); \quad T=T_w H(t) \tag{31e}$$

Problem 2:
At far field ($r\to\infty$)

$$\sigma_{zz}=-S_z+[\nu'(S_x+S_y)+(\alpha'-2\nu'\alpha)p_0+(\beta^{s'}-2\nu'\beta^s)T_0] \tag{32a}$$

$$\sigma_{xx}=\sigma_{yy}=\tau_{xy}=\tau_{yz}=\tau_{xz}=p=T=0 \tag{32b}$$

At borehole wall ($r=R$)

$$\sigma_{rr}=\tau_{r\theta}=\tau_{rz}=p=T=0 \tag{32c}$$

Problem 3:
At far field ($r\to\infty$)

$$\sigma_{xx}=\sigma_{yy}=\sigma_{zz}=\tau_{xy}=p=T=0 \tag{33a}$$

$$\tau_{xy}=-S_{xy}; \quad \tau_{yz}=-S_{yz} \tag{33b}$$

At the borehole wall ($r=R$)

$$\sigma_{rr}=\tau_{r\theta}=\tau_{rz}=p=T=0 \tag{33c}$$

Table 1 Material parameters

Parameter	Units	Value
Elastic modulus (E)	GPa	9.474
Poisson's ratio (ν)	⋯	0.24
Grain bulk modulus (K_s)	GPa	27.5
Biot's modulus (M)	GPa	8.875
Permeability (k)	md	5.0×10^{-5}
Fluid viscosity (μ)	MPa·s	10^{-9}
Heat diffusivity·(c_h)	m^2/day	0.138 24
Linear expansion coefficient (solid skeleton, α^s)	/°C	6.0×10^{-6}
Volumetric expansion coefficient (fluid, α^s)	/°C	3.0×10^{-4}
Porosity (ϕ)	⋯	0.14

In addition, the solution for the modified plane strain problem is obtained by a decomposition of the boundary conditions into three contributing loading modes [32]. Of these, mode 1 accounts for the hydrostatic part of the boundary stresses, mode 2 accounts for both the pore pressure and temperature perturbations, and mode 3 takes into account the deviant part of the boundary stresses. Only modes 2 and 3 are time dependent, in that mode 2 is characterized by coupling between the pore fluid and heat diffusion processes. Although mode 3 shows characteristics of full poroelastic coupling it is still not affected by temperature perturbations. The boundary conditions at the borehole wall are as follows:

Mode 1:

$$\sigma_{rr}^{(1)}=P_0-p_w; \quad \sigma_{r\theta}^{(1)}=0; \quad p^{(1)}=0; \quad T^{(1)}=0; \tag{34a}$$

Mode 2:

$$\sigma_{rr}^{(2)}=0; \quad \sigma_{r\theta}^{(2)}=0; \quad p^{(2)}=(p_w-p_0); \quad T^{(2)}=(T_w-T_0) \tag{34b}$$

Mode 3:

$$\sigma_{rr}^{(3)}=-S_0\cos 2(\theta-\theta_r); \quad \sigma_{r\theta}^{(3)}=S_0\sin 2(\theta-\theta_r);$$
$$p^{(3)}=0; \quad T^{(3)}=0 \tag{34c}$$

where θ_r is given by

$$\theta_r=\tfrac{1}{2}\tan^{-1}[2S_{xy}/(S_x+S_y)] \tag{35}$$

The complete solution for the inclined borehole problem is obtained by a superposition and is given in the Appendix.

Numerical Examples

The solutions developed in the previous section are applied to assess the effect of the anisotropic parameters on the stress and pore pressure distribution in the vicinity of the borehole. The borehole orientation is given by two angles as shown in Fig. 1(*a*) which are the azimuth, $\varphi_y=30$ deg, and the inclination $\varphi_z=60$ deg. Comparisons with the corresponding isotropic porothermoelastic and the isotropic poroelastic cases are made to highlight the anisotropy effects on the results obtained.

A borehole of radius 0.1 m is assumed to be drilled in the formation characterized by in situ stress and pore pressure gradients given as: $S_{x'}=25$ kPa/m, $S_{y'}=22$ kPa/m, $S_{z'}=29$ kPa/m, $p_0=9.8$ kPa/m. A section at a depth of 1000 m is analyzed where the formation temperature is assumed to be $T_0=125$°C. The borehole is assumed to be filled with a fluid maintained at a constant pressure given by $p_w=12.0$ MPa. The material properties used in the analysis are given in Table 1.

The degree of anisotropy of material parameters is modeled by selecting appropriate values for the ratios E/E', ν/ν', and $\alpha^s/\alpha^{s'}$. Numerical results are presented in Figs. 2–17, in which negative values of stresses are presented indicating that compression is denoted positive.

Effect of Temperature. The effect of temperature on the pore pressure and stress distributions is examined for the transversely

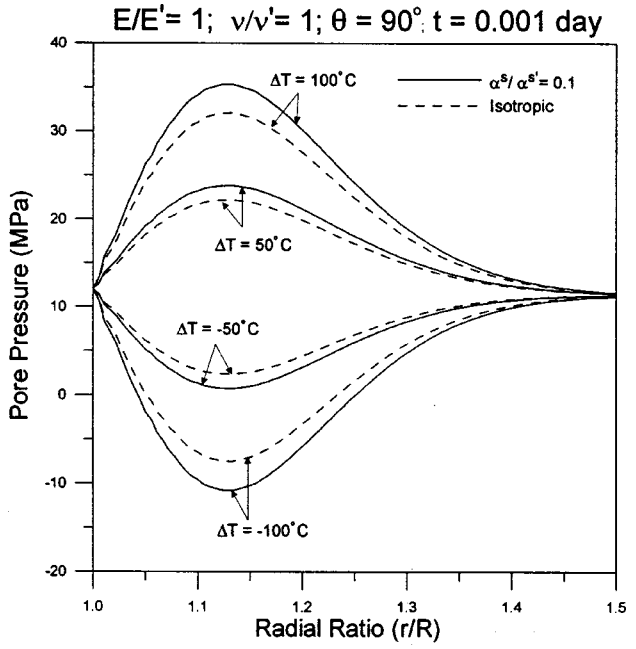

Fig. 2 Pore pressure varying with r/R along θ=90 deg at t=0.001 day for different values of ΔT

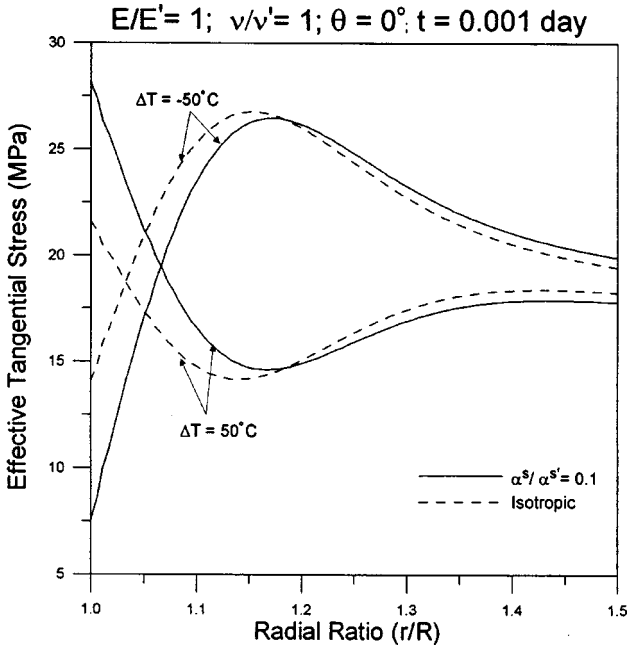

Fig. 4 Effective tangential stress varying with r/R along θ=90 deg at t=0.001 day for different values of ΔT

isotropic material and compared with the isotropic case. Only the anisotropy of thermic coefficients is modeled by fixing ratios for $E/E'=1$ and $\nu/\nu'=1$ and varying $\alpha^s/\alpha^{s'}$. The difference between the wellbore fluid and the formation temperature, ΔT, is varied where $\Delta T=T_w-T_0$. All the results shown in this regard are for a short time interval, i.e., $t=0.001$ day. Figures 2 and 3 show the pore pressure and the effective radial stress distributions, respectively, as a function of the radial distance along the θ=90 deg direction. Figure 2 shows that the temperature perturbation induces a higher pore pressure close the to borehole wall for the cases where ΔT is positive or when the wellbore fluid is at a higher temperature than the formation. On the other hand, a negative value of ΔT results in a reduction of the pore pressure. Also, both effects are more pronounced for the transversely isotropic case. The induced pore pressure (positive or negative) leads to a modification of the effective radial stresses. As presented in Fig. 3, the effective radial stresses are tensile when the wellbore fluid is at a higher temperature than the formation with the tensile magnitude being higher in the transversely isotropic material. In the case of a lower wellbore fluid temperature, the effective radial stresses are compressive in nature. Again, the compressive magnitude is higher for the transversely isotropic case. Figure 4 shows the effective tangential stress as a function of the radial distance along the θ=0 deg direction. As seen from Fig. 4, higher effective tangential stresses are observed when the wellbore fluid has a higher temperature. With a lower wellbore fluid temperature, the effective tangential stresses are reduced. This is also seen clearly in Fig. 5, which presents the variation of the effective tangential stresses around the borehole at $r/R=1$. Figure 5 has been generated using the data given by Li et al. [34] and is given in Table 2. However, as seen from Fig. 5, a lower wellbore fluid temperature leads to significant lowering of the effective tangential stress for the transversely isotropic case.

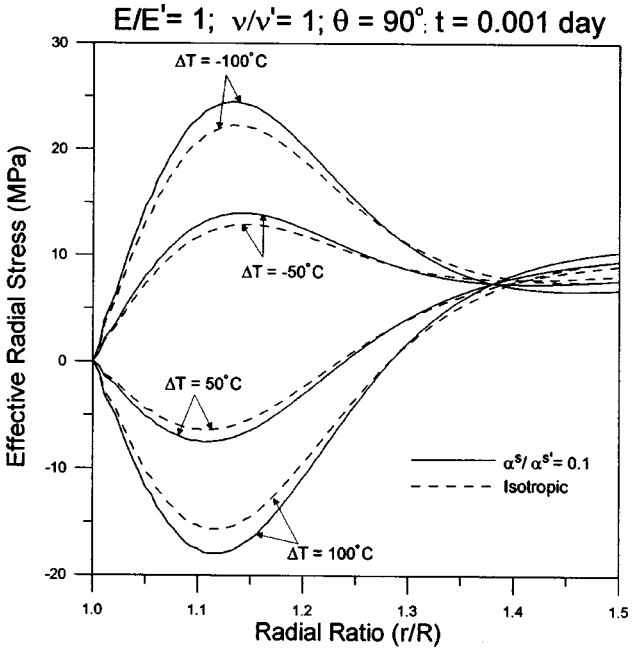

Fig. 3 Effective radial stress varying with r/R along θ=90 deg at t=0.001 day for different values of ΔT

Effect of Anisotropy of Thermic Coefficients. To evaluate the effect of the anisotropic nature of the thermic coefficients on the stress and pore pressure distributions, we fix the ratios for $E/E'=1$ and $\nu/\nu'=1$ and vary $\alpha^s/\alpha^{s'}$. In other words, we assume that material anisotropy is only because of a different $\alpha^{s'}$ value in the transverse direction. Notice that the above choice results only in the variation of values for the thermic coefficients β^s, $\beta^{s'}$, and β^{sf} with all other material coefficients (M_{ijkl}'s, α, and α') assuming their values as in the isotropic case. Data given in Table 1 are used for the analysis. The temperature difference between the wellbore fluid and the formation is assumed to be $\Delta T=50°C$. Again, results are shown for a short time interval, i.e., $t=0.001$ day.

Figures 6 and 7 show the pore pressure profile as a function of the radial distance along the θ=90 deg direction. In Fig. 6 results are shown for lower thermic coefficient ratios $\alpha^s/\alpha^{s'}=0.1$, 0.5 along with the corresponding isotropic porothermoelastic and po-

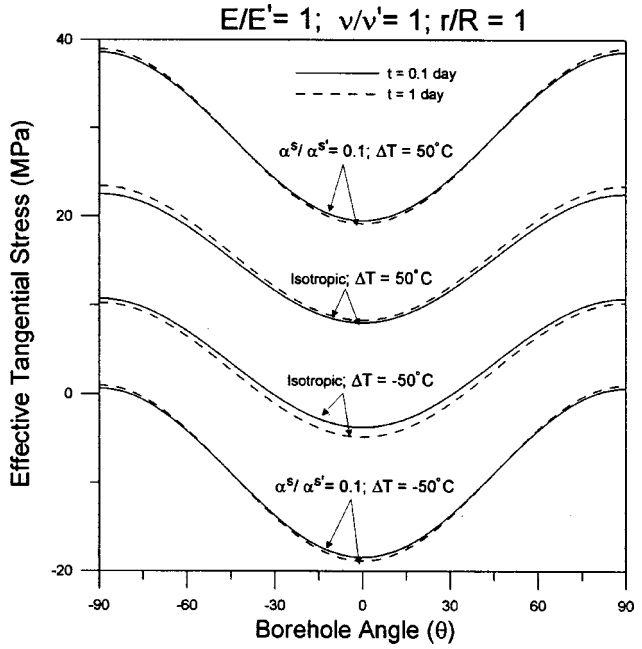

Fig. 5 Effective tangential stress around the wellbore at $r/R=1$ for different values of ΔT and $\alpha^s/\alpha^{s'}$. Curves generated using data given by Li et al., 1998 (Table 2).

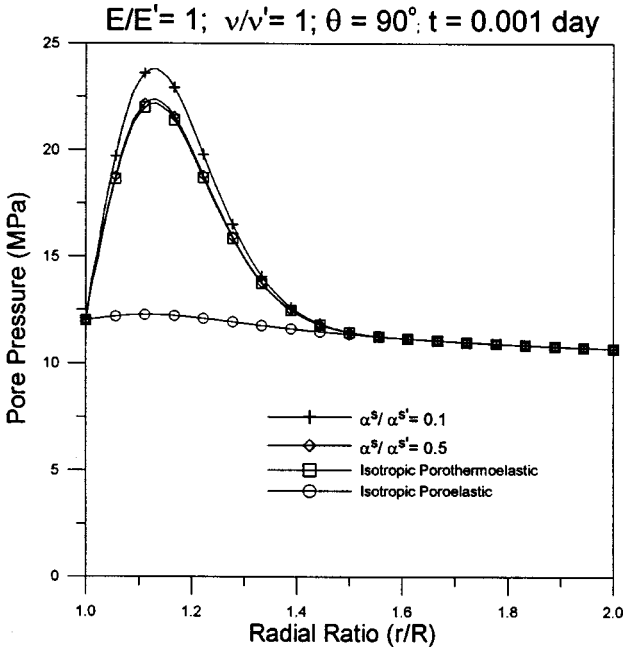

Fig. 6 Pore pressure varying with r/R along $\theta=90$ deg at $t=0.001$ day

roelastic cases. On the other hand, Fig. 7 show results corresponding to higher values of thermic coefficient ratios, i.e., $\alpha^s/\alpha^{s'}=2.0$, 5.0. First, the pore pressure profile in the poroelastic case exhibits the well-known Mandel–Cryer effect. In addition, all the porothermoelastic cases show an increased value of the pore pressure close to the region near the borehole wall.

Figures 8 and 9 show, respectively, the effective radial and tangential stress profiles for the two lower values of the thermic coefficient ratios, i.e., $\alpha^s/\alpha^{s'}=0.1$, 0.5. Tensile effective radial stresses are observed in the vicinity of the borehole which is a natural consequence of the high induced pore pressure as discussed above. Again, as observed in the earlier cases, the tensile magnitude of the stress is more predominant for the case with lower $\alpha^s/\alpha^{s'}$ ratio. In contrast, lower $\alpha^s/\alpha^{s'}$ ratios result in more compressive tangential stresses as can be seen from Fig. 9. However, at a short distance inside the formation, the effective tangential stresses are lowered, which may be again attributed to the effect of the induced pore pressure. The aforementioned observations can be directly linked to the effect of the $\alpha^s/\alpha^{s'}$ ratios on values of β^s, $\beta^{s'}$, and β^{sf}. A simple calculation shows that, for lower values of the $\alpha^s/\alpha^{s'}$ ratio ($\alpha^s/\alpha^{s'}<1.0$), the thermic coefficients β^s, $\beta^{s'}$, and β^{sf} assume higher values. As a result, a higher magnitude of the pore pressure is induced and the total stresses are more compressive.

Next, we present results in the form of stress clouds to illustrate the shear failure potential. The "stress clouds" represent the amalgamation of the effective radial, tangential, and shear stresses presented in the $\sqrt{J_2}-S_p$ space, where $\sqrt{J_2}$ is the mean shear stress given by

Table 2 Material parameters (Li et al., 1998)

Parameter	Units	Value
Shear modulus (G)	GPa	8.88
Poisson's ratio (ν)	···	0.189
Undrained poisson's ratio (ν_u)	···	0.314
Skempton's coefficient (B)	GPa	0.596
Permeability (k)	md	5.0×10^{-5}
Fluid viscosity (μ)	MPa·s	10^{-9}
Heat diffusivity·(c_h)	m^2/s	1.6×10^{-6}
Volumetric expansion coefficient (solid skeleton, α^s)	/°C	18.0×10^{-6}
Volumetric expansion coefficient (fluid, α^s)	/°C	3.0×10^{-4}
Porosity (ϕ)	···	0.14
Wellbore fluid pressure	MPa	13.5

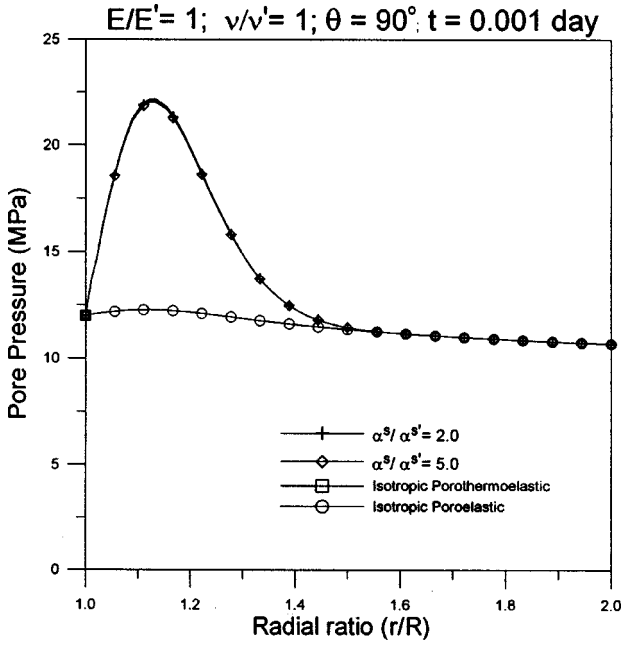

Fig. 7 Pore pressure varying with r/R along $\theta=90$ deg at $t=0.001$ day

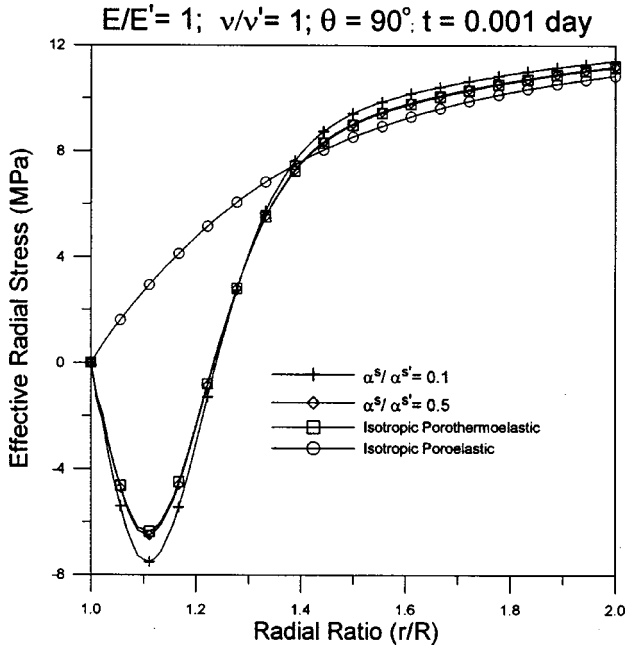

Fig. 8 Effective radial stress varying with r/R along θ=90 deg at t=0.001 day

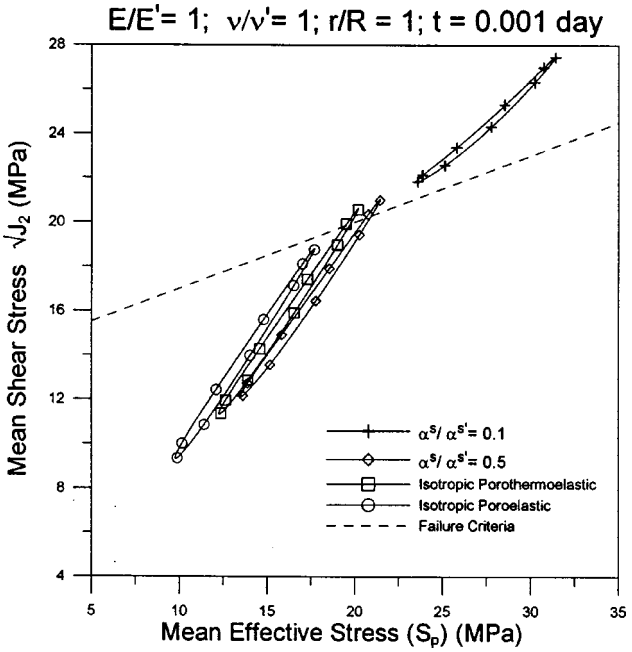

Fig. 10 Stress clouds at r/R=1 and t=0.001 day

$$J_2=\tfrac{1}{6}[(\sigma_{rr}-\sigma_{\theta\theta})^2+(\sigma_{\theta\theta}-\sigma_{zz})^2+(\sigma_{zz}-\sigma_{rr})^2]+\sigma_{r\theta}^2+\sigma_{rz}^2+\sigma_{\theta z}^2 \tag{36}$$

and S_p is the mean effective stress given by

$$S_p=-\frac{\sigma_{rr}+\sigma_{\theta\theta}+\sigma_{zz}}{3}-p \tag{37}$$

The stress cloud is obtained by evaluating pairs of $(S_p, \sqrt{J_2})$ by varying the angle around the borehole, θ for a fixed radial distance and time [32]. The stress cloud concept is used in conjunction with the Drucker–Prager criterion for a shear failure analysis. The Drucker–Prager criterion can be expressed as

$$\sqrt{J_2}=3AS_p+D \tag{38}$$

where A and D are positive material constants. Values of $A=0.1$ and $D=14$ MPa are chosen to represent the failure envelope.

Figure 10 shows the stress clouds at the borehole wall, i.e., $r/R=1.0$. It is seen that, for a lower $\alpha^s/\alpha^{s'}$ ratio, the stress cloud moves to the right and higher, pushing it outside the failure envelope. At the borehole wall, the effective radial stresses are always zero. However, there is an increase in the effective tangential stress and the effective axial stress for the lower $\alpha^s/\alpha^{s'}$ ratio. This results in a higher difference between the stresses which causes the mean shear stress, $\sqrt{J_2}$, to increase. With higher effective tangential and axial stresses, the mean effective stress, S_p, is naturally higher. Hence, the stress cloud moves higher and to the right for the lower $\alpha^s/\alpha^{s'}$ ratio. Figure 11 shows the stress clouds at a fractional distance inside the formation given by $r/R=1.1$. The relative magnitudes of the stresses are still quite different for the lower $\alpha^s/\alpha^{s'}$ ratio, resulting in a cloud which is partially outside the failure envelope. Again, Figs. 10 and 11 show that higher thermal expansion coefficients in the transverse direction lead to a higher shear failure potential. Also shown in Fig. 12 are the variations of the effective tangential stresses as a function of the angle around the borehole, θ, at the borehole wall. The tangential stress is more compressive for lower values of the $\alpha^s/\alpha^{s'}$ ratio. A higher wellbore pressure would thus be required to produce tensile zones, indicating that a higher thermal coefficient in the transverse direction results in decreasing the fracturing failure potential.

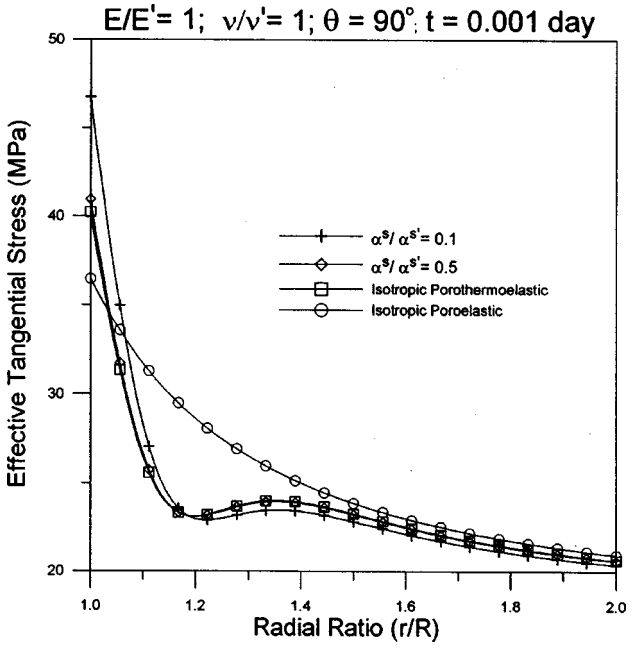

Fig. 9 Effective tangential stress varying with r/R along θ=90 deg at t=0.001 day

Time-Dependent Effects. It is interesting to show the behavior of stresses and pore pressure as time progresses. In Figs. 13–15 we show their variation with radial distance, along the θ=90 deg direction for three time intervals, $t=0.001$, 0.01, and 0.1 day. Also, results are shown for two values of the thermal expansion coefficient ratios, i.e., $\alpha^s/\alpha^{s'}=0.1$ and 1.0. It is seen from Fig. 13 that the magnitude of the induced pore pressure

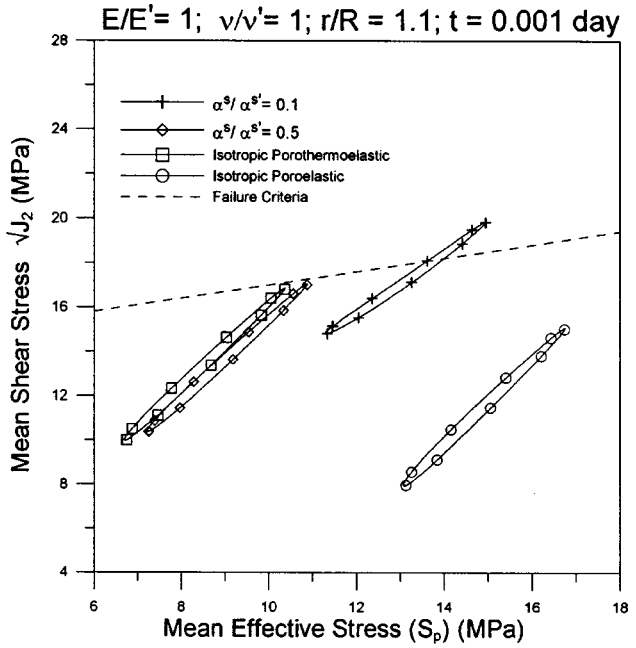

Fig. 11 Stress clouds at $r/R=1$ and $t=0.001$ day

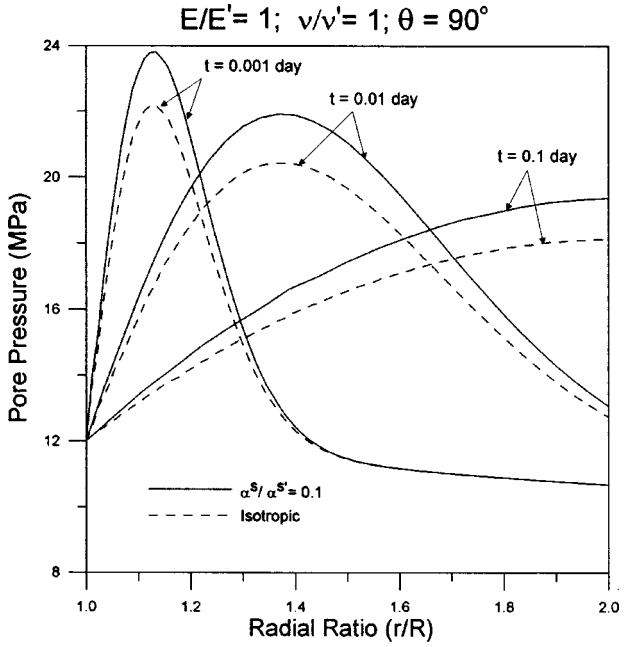

Fig. 13 Pore pressure varying with r/R for $\alpha_m/\alpha'_m=0.1, 1.0$, for $t=0.001$, 0.01, and 0.1 day

progressively decreases with time. In addition, the location of the maximum pore pressure gradually moves into the formation and away from the borehole wall. The magnitude of the pore pressure for the lower $\alpha^s/\alpha^{s'}$ is, however, always higher. It is seen from Fig. 14 that with the passage of time effective radial stresses in the vicinity of the borehole change from tensile to compressive in nature as a result of the diffusion process. Correspondingly, as time progresses the effective tangential stresses become more compressive, as can be seen from Fig. 15. It may be expected that, as the induced pore pressure front progresses into the formation, it results in lowering the effective stresses, indicating that the potential shear failure zone gradually shifts into the formation.

Combined Anisotropic Effects. The combined effect of the anisotropy of elastic parameters and the thermal expansion coefficient ratios is analyzed in Figs. 16–18. The pore pressure profiles for four sets of values of the E/E', ν/ν' and $\alpha^s/\alpha^{s'}$ ratios are shown in Fig. 16. It can be seen that for the two curves where $E/E'=2$, $\nu/\nu'=2$, the pore pressure induced is higher for the case when $\alpha^s/\alpha^{s'}=0.1$ as compared to that for the $\alpha^s/\alpha^{s'}=0.5$. In contrast, when $E/E'=0.5$, $\nu/\nu'=0.5$, the pore pressure is lower for the case where $\alpha^s/\alpha^{s'}=0.1$ than for $\alpha^s/\alpha^{s'}=0.5$. A similar observation is made about the tensile nature of the effective radial

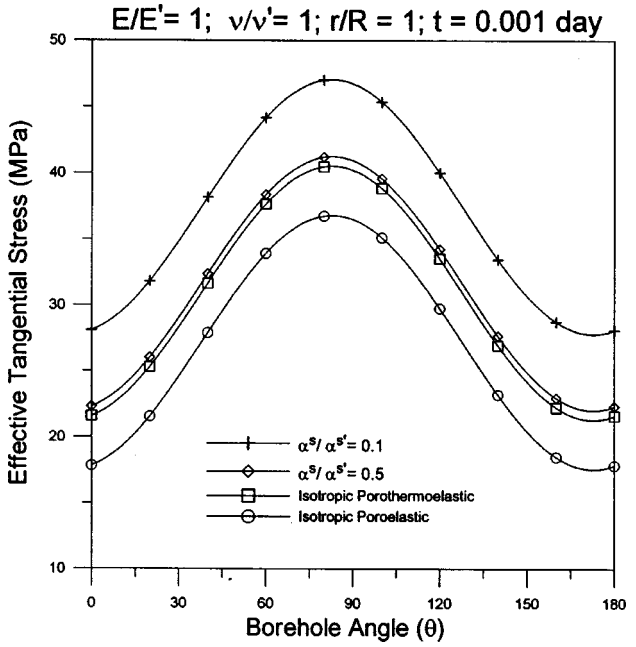

Fig. 12 Effective tangential stress varying with θ at $r/R=1$ and $t=0.001$ day

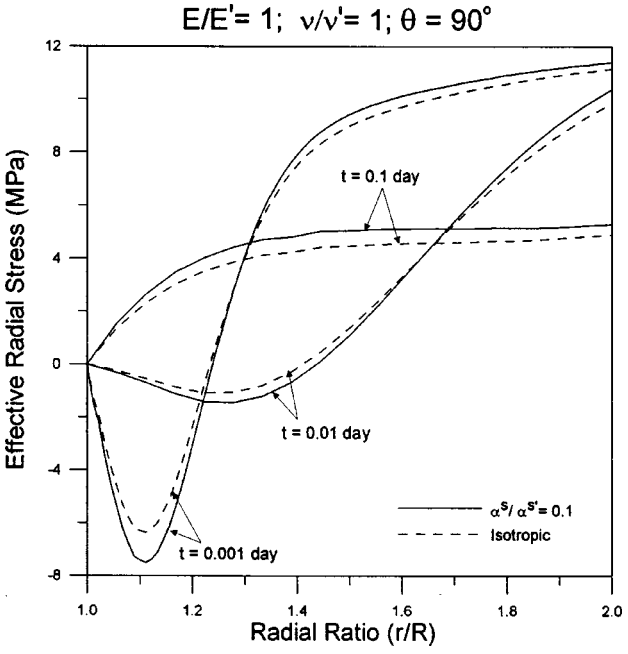

Fig. 14 Effective radial stress varying with r/R for $\alpha_m/\alpha'_m=0.1, 1.0$, for $t=0.001$, 0.01, and 0.1 day

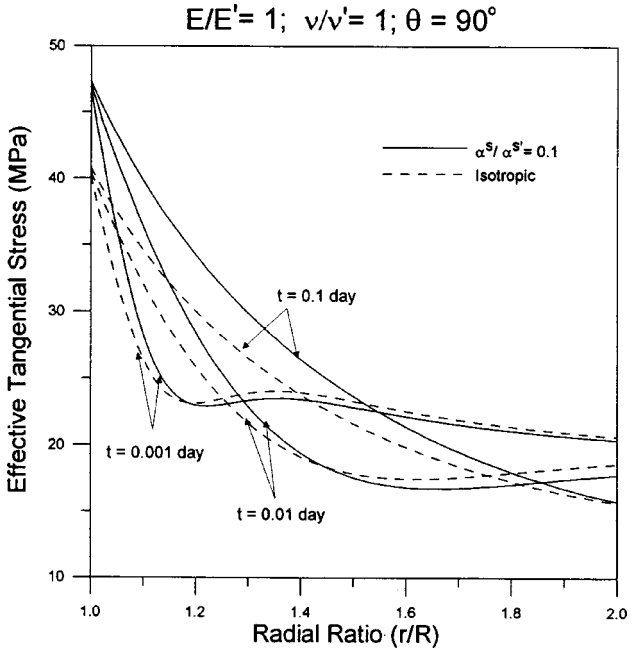

Fig. 15 Effective tangential stress varying with r/R for α_m/α'_m=0.1, 1.0, for t=0.001, 0.01, and 0.1 day

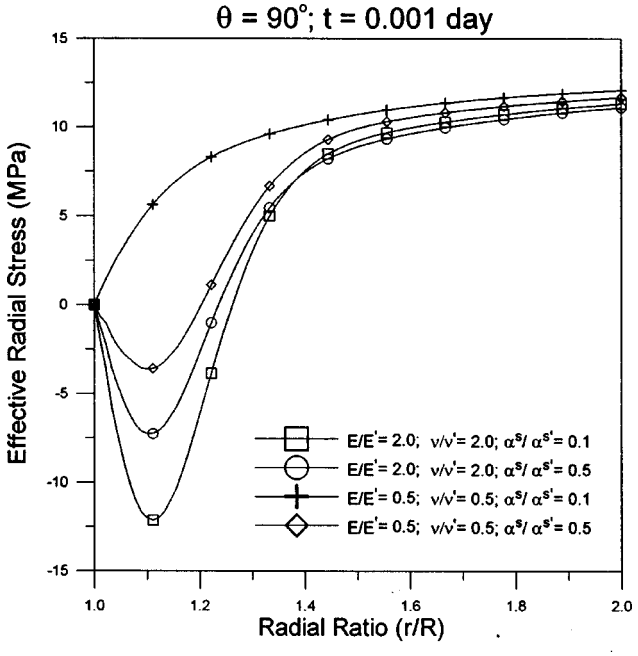

Fig. 17 Effective radial stress varying with r/R at t=0.001 day for different combinations of E/E', ν/ν', and α_m/α'_m

stresses, shown in Fig. 17. On the other hand, the effective tangential stress shown in Fig. 18 is most compressive for lower ratios of E/E', ν/ν', and $\alpha^s/\alpha^{s'}$. The combined effect of the anisotropy of both the material and thermal expansion coefficients results in complex behavior patterns. A consistent inference which relates the change in values for these ratios to behavior of the stresses and pore pressure may be difficult to draw. However, noting that a change in these ratios results in a corresponding modification of the values for β^s, $\beta^{s'}$, and β^{sf}, a fair prediction is plausible.

Conclusions

The solution for the inclined borehole problem in a transversely isotropic poroelastic medium under nonisothermal conditions has been presented in this paper. A superposition scheme, involving decomposition of the complex problem along with its boundary conditions into simpler problems which can be solved easily, has been used to arrive upon the solution. A parametric analysis has been presented to study the material anisotropy effect on the stress and pore pressure profiles.

The temperature difference leads to a modification of both the pore pressure and stress distributions. The effect of the anisotropy

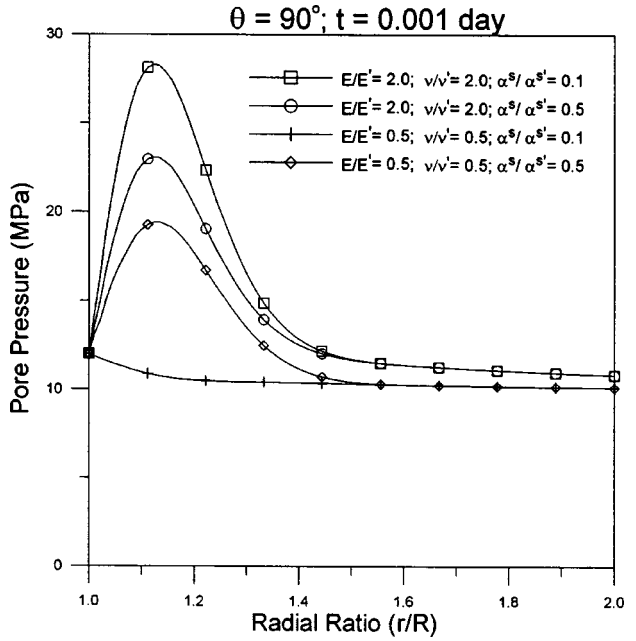

Fig. 16 Pore pressure varying with r/R at t=0.001 day for different combinations of E/E', ν/ν', and α_m/α'_m

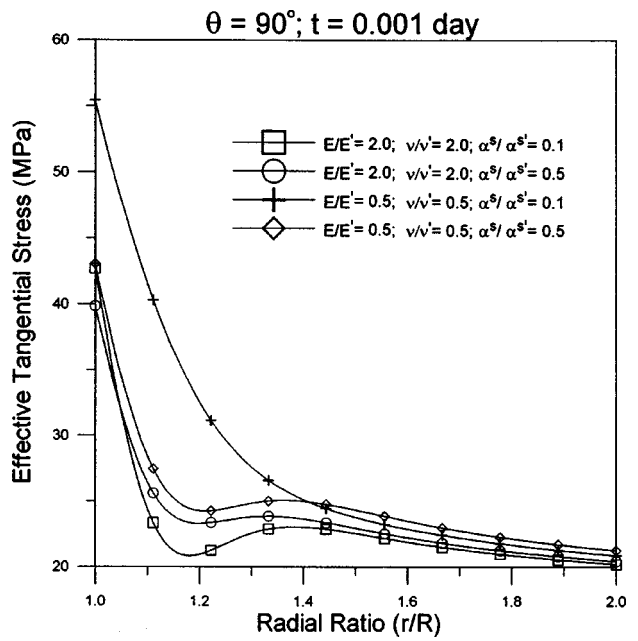

Fig. 18 Effective tangential stress varying with r/R at t =0.001 day for different combinations of E/E', ν/ν', and α_m/α'_m

of thermic coefficients has been studied varying the thermal expansion coefficients in the isotropic and transverse directions while keeping the mechanical parameters isotropic. It was found that the effects on the pore pressure and stress profiles are more pronounced when the material has a higher thermal expansion coefficient in the transverse direction. In contrast, the stress and pore pressure responses are more or less comparable to the isotropic case when the thermal expansion coefficients are lower in the transverse direction. The time-dependent variation of the induced pore pressure is characterized by a front which moves into the formation as time progresses. The effect of anisotropy of mechanical parameters has been studied varying E/E' and ν/ν'. It is interesting to note that for ratios of E/E', $\nu/\nu'>1$, the ratios of the thermal expansion coefficients affect the stress and pore pressure distributions in a manner similar to the case when the mechanical parameters are isotropic. On the other hand, when E/E', $\nu/\nu'<1$, the trend of these results (i.e., effect of $\alpha^s/\alpha^{s'}$) is reversed.

Again, it must be noted that applicability of the analytical solution may seem limited for the case where the isotropic plane is perpendicular to the borehole axis. Nevertheless, it serves as a unique tool in both understanding the underlying phenomena, and, validation of numerical analyses in which some of the assumptions may be relaxed subsequently [35,36].

Acknowledgments

The authors would like to thank Dr. Mazen Kanj and Dr. Rajesh Nair for the discussion pertaining to the results and constructive suggestions in preparing this manuscript. The financial support from the Rock Mechanics Consortium, at the PoroMechanics Institute, is also acknowledged.

Appendix

Transversely Isotropic Borehole Solution. The complete solution for the inclined borehole problem in a transversely isotropic medium and an isotropic medium are given.

$$\sigma_{rr}=-P_0+S_0\cos 2(\theta-\theta_r)+\sigma_{rr}^{(1)}+\sigma_{rr}^{(2)}+\sigma_{rr}^{(3)} \quad (A1a)$$

$$\sigma_{\theta\theta}=-P_0-S_0\cos 2(\theta-\theta_r)+\sigma_{\theta\theta}^{(1)}+\sigma_{\theta\theta}^{(2)}+\sigma_{\theta\theta}^{(3)} \quad (A1b)$$

$$\sigma_{zz}=-S_z+[\nu'(S_x+S_y)+(\alpha'-2\nu'\alpha)p_0+(\beta'-2\nu'\beta)T_0]+\nu'(\sigma_{rr}+\sigma_{\theta\theta})-(\alpha'-2\nu'\alpha)p-(\beta'-2\nu'\beta)T \quad (A1c)$$

$$\sigma_{r\theta}=-P_0+S_0\sin 2(\theta-\theta_r)+\sigma_{r\theta}^{(3)} \quad (A1d)$$

$$\sigma_{rz}=-(S_{xz}\cos\theta+S_{yz}\sin\theta)[1-(R^2/r^2)] \quad (A1e)$$

$$\sigma_{\theta z}=(S_{xz}\sin\theta+S_{yz}\cos\theta)[1+(R^2/r^2)] \quad (A1f)$$

$$p=p_0+p^{(2)}+p^{(3)} \quad (A1g)$$

$$T=T_0+T^{(2)} \quad (A1h)$$

where $\sigma_{rr}^{(1)}$, $\sigma_{rr}^{(2)}$, $\sigma_{rr}^{(3)}$, $\sigma_{\theta\theta}^{(1)}$, $\sigma_{\theta\theta}^{(2)}$, $\sigma_{\theta\theta}^{(3)}$, $\sigma_{r\theta}^{(3)}$, $p^{(2)}$, $p^{(3)}$, and $T^{(2)}$ are obtained by solving the modified plane strain problem as indicated earlier. In the above, θ_r, P_0, and S_0 are given by

$$\theta_r=\tfrac{1}{2}\tan^{-1}[2S_{xy}/(S_x+S_y)] \quad (A2a)$$

$$P_0=(S_x+S_y)/2 \quad (A2b)$$

$$S_0=0.5\sqrt{(S_x-S_y)^2+4S_{xy}^2} \quad (A2c)$$

The expressions for $\sigma_{rr}^{(1)}$, $\sigma_{rr}^{(2)}$, $\sigma_{rr}^{(3)}$, $\sigma_{\theta\theta}^{(1)}$, $\sigma_{\theta\theta}^{(2)}$, $\sigma_{\theta\theta}^{(3)}$, $\sigma_{r\theta}^{(3)}$, $p^{(2)}$, $p^{(3)}$, and $T^{(2)}$ are obtained as follows [32,37]:

Solutions for Mode 1:

$$\sigma_{rr}^{(1)}=H(t)[P_0-p_w]\left(\frac{R^2}{r^2}\right) \quad (A3a)$$

$$\sigma_{\theta\theta}^{(1)}=-H(t)[P_0-p_w]\left(\frac{R^2}{r^2}\right) \quad (A3b)$$

Solutions for mode 2 and mode 3 are obtained in the Laplace domain and are inverted to the time-domain using the Stehfest algorithm [37].

Solutions for Mode 2:

$$s\tilde{T}^{(2)}=(T_w-T_0)\Phi(\omega) \quad (A4a)$$

$$s\tilde{p}^{(2)}=G_1\Phi(\xi)+G_2\Phi(\omega) \quad (A4b)$$

$$s\tilde{\sigma}_{rr}^{(2)}=\alpha\left(1-\frac{M_{12}}{M_{11}}\right)\{\mathsf{F}_1\Psi(\xi)+\mathsf{F}_2\Psi(\omega)\}+\beta^s\left(1-\frac{M_{12}}{M_{11}}\right)\{(T_w-T_0)\Psi(\omega)\} \quad (A4c)$$

$$s\tilde{\sigma}_{\theta\theta}^{(2)}=-\alpha\left(1-\frac{M_{12}}{M_{11}}\right)\{\mathsf{F}_1\Omega(\xi)+\mathsf{F}_2\Omega(\omega)\}-\beta^s\left(1-\frac{M_{12}}{M_{11}}\right)\{(T_w-T_0)\Omega(\omega)\} \quad (A4d)$$

Solutions for Mode 3:

$$\tilde{p}^{(3)}=\frac{S_0}{s}\left(\frac{c_f}{2G\kappa}C_1\mathrm{K}_2(\xi r)+A_1C_2\frac{R^2}{r^2}\right)\cos 2(\theta-\theta_r) \quad (A5a)$$

$$\tilde{\sigma}_{rr}^{(3)}=\frac{S_0}{s}\left[A_1C_1\left(\frac{1}{\xi r}\mathrm{K}_1(\xi r)+\frac{6}{(\xi r)^2}\mathrm{K}_2(\xi r)\right)-A_2C_2\frac{R^2}{r^2}-3C_3\frac{R^4}{r^4}\right]\cos 2(\theta-\theta_r) \quad (A5b)$$

$$\tilde{\sigma}_{\theta\theta}^{(3)}=\frac{S_0}{s}\left[-A_1C_1\left(\frac{1}{\xi r}\mathrm{K}_1(\xi r)\left(1+\frac{6}{(\xi r)^2}\right)\mathrm{K}_2(\xi r)\right)+3C_3\frac{R^4}{r^4}\right]\cos 2(\theta-\theta_r) \quad (A5c)$$

$$\tilde{\tau}_{r\theta}^{(3)}=\frac{S_0}{s}2A_1C_1\left(\frac{1}{\xi r}\mathrm{K}_1(\xi r)+\frac{3}{(\xi r)^2}\mathrm{K}_2(\xi r)\right)-\frac{A_2}{2}C_2\frac{R^2}{r^2}-3C_3\frac{R^4}{r^4}\sin 2(\theta-\theta_r) \quad (A5d)$$

where K_n is the modified Bessel function of the second kind of order n. In the above

$$\Phi(x)=\left[\frac{\mathrm{K}_0(xr)}{\mathrm{K}_0(xR)}\right] \quad (A6a)$$

$$\Psi(x)=\left[\frac{\mathrm{K}_1(xr)}{xr\mathrm{K}_0(xR)}-\frac{R\mathrm{K}_1(xR)}{xr^2\mathrm{K}_0(xR)}\right] \quad (A6b)$$

$$\Omega(x)=\left[\frac{\mathrm{K}_1(xr)}{xr\mathrm{K}_0(xR)}-\frac{R\mathrm{K}_1(xR)}{xr^2\mathrm{K}_0(xR)}+\frac{\mathrm{K}_0(xr)}{\mathrm{K}_0(xR)}\right] \quad (A6c)$$

$$\mathsf{F}_1=\left[(p_w-p_0)-\left(\frac{c_{hf}}{(1-c_f/c_h)}\right)(T_w-T_0)\right] \quad (A6d)$$

$$\mathsf{F}_2=\left(\frac{c_{hf}}{(1-c_f/c_h)}\right)(T_w-T_0) \quad (A6e)$$

$$\omega=\sqrt{\frac{s}{c_h}};\quad \xi=\sqrt{\frac{s}{c_f}} \quad (A6f)$$

The constants C_1, C_2, C_3

$$C_1=\frac{4}{2A_1(B_3-B_2)-A_2B_1} \tag{A7a}$$

$$C_2=-\frac{4B_1}{2A_1(B_3-B_2)-A_2B_1} \tag{A7b}$$

$$C_3=\frac{2A_1(B_2+B_3)+3A_2B_1}{3[2A_1(B_3-B_2)-A_2B_1]} \tag{A7c}$$

in which

$$A_1=\frac{\alpha M}{M_{11}+\alpha^2 M} \tag{A8a}$$

$$A_2=\frac{M_{11}+M_{12}+2\alpha^2 M}{M_{11}+\alpha^2 M} \tag{A8b}$$

$$B_1=\frac{M_{11}}{2G\alpha}\mathrm{K}_2(\xi R) \tag{A8c}$$

$$B_2=\frac{1}{\xi R}\mathrm{K}_1(\xi R)+\frac{6}{(\xi R)^2}\mathrm{K}_2(\xi R) \tag{A8d}$$

$$B_3=2\left(\frac{1}{\xi R}\mathrm{K}_1(\xi R)+\frac{3}{(\xi R)^2}\mathrm{K}_2(\xi R)\right) \tag{A8e}$$

Isotropic Borehole Solution

Complete solution for the inclined borehole in an isotropic material is obtained using the same decomposition scheme and Eqs. (*A*1*a*)–(*A*1*h*), with the added condition that $\alpha=\alpha'$ and $\beta^s=\beta^{s'}$. Solutions for $\sigma_{rr}^{(1)}$, $\sigma_{rr}^{(2)}$, $\sigma_{rr}^{(3)}$, $\sigma_{\theta\theta}^{(1)}$, $\sigma_{\theta\theta}^{(2)}$, $\sigma_{\theta\theta}^{(3)}$, $\sigma_{r\theta}^{(3)}$, $p^{(2)}$, $p^{(3)}$, and $T^{(2)}$ for the inclined borehole in the isotropic medium were obtained by Li et al. [34]. Their solutions have been corrected for some of the typographical errors and reproduced for clarification below.

Solutions for Mode 1:

Solutions for $\sigma_{rr}^{(1)}$ and $\sigma_{\theta\theta}^{(1)}$ are the same as given in Eqs. (*A*3*a*) and (*A*3*b*).

Solutions for Mode 2:

$$s\tilde{T}^{(2)}=(T_w-T_0)\Phi(\omega) \tag{A9a}$$

$$s\tilde{p}^{(2)}=\mathsf{F}_1\Phi(\xi)+\mathsf{F}_2\Phi(\omega) \tag{A9b}$$

$$s\tilde{\sigma}_{rr}^{(2)}=\alpha\left(\frac{1-2\nu}{1-\nu}\right)\{\mathsf{F}_1\Psi(\xi)+\mathsf{F}_2\Psi(\omega)\}+\beta^s\left(\frac{1-2\nu}{1-\nu}\right)\{(T_w-T_0)\Psi(\omega)\} \tag{A9c}$$

$$s\tilde{\sigma}_{\theta\theta}^{(2)}=-\alpha\left(\frac{1-2\nu}{1-\nu}\right)\{\mathsf{F}_1\Omega(\xi)+\mathsf{F}_2\Omega(\omega)\}-\beta^s\left(\frac{1-2\nu}{1-\nu}\right)\{(T_w-T_0)\Omega(\omega)\} \tag{A9d}$$

The functions $\Phi(x)$, $\Psi(x)$, and $\Omega(x)$, F_1, F_2 are as defined in Eqs. (*A*6*a*)–(*A*6*c*).

Solutions for Mode 3:

$$\tilde{p}^{(3)}=\frac{S_0}{s}\left[\frac{B^2(1-\nu)(1+\nu_u)^2}{9(1-\nu_u)(\nu_u-\nu)}C_1\mathrm{K}_1(\xi r)+\frac{B(1+\nu_u)}{3(1-\nu_u)}C_2\frac{R^2}{r^2}\right]\cos 2(\theta-\theta_r) \tag{A10a}$$

$$\tilde{\sigma}_{rr}^{(3)}=\frac{S_0}{s}\left[\frac{B(1+\nu_u)}{3(1-\nu_u)}C_1\left(\frac{1}{\xi r}\mathrm{K}_1(\xi r)+\frac{6}{(\xi r)^2}\mathrm{K}_2(\xi r)\right)-\frac{1}{1-\nu_u}C_2\frac{R^2}{r^2}-3C_3\frac{R^4}{r^4}\right]\cos 2(\theta-\theta_r) \tag{A10b}$$

$$\tilde{\sigma}_{\theta\theta}^{(3)}=\frac{S_0}{s}\left[-\frac{B(1+\nu_u)}{3(1-\nu_u)}C_1\left(\frac{1}{\xi r}\mathrm{K}_1(\xi r)\left[1+\frac{6}{(\xi r)^2}\right]\mathrm{K}_2(\xi r)\right)+3C_3\frac{R^4}{r^4}\right]\cos 2(\theta-\theta_r) \tag{A10c}$$

$$\tilde{\tau}_{r\theta}^{(3)}=\frac{S_0}{s}\left[\frac{2B(1+\nu_u)}{3(1-\nu_u)}C_1\left(\frac{1}{\xi r}\mathrm{K}_1(\xi r)+\frac{3}{(\xi r)^2}\mathrm{K}_2(\xi r)\right)-\frac{1}{2(1-\nu_u)}C_2\frac{R^2}{r^2}-3C_3\frac{R^4}{r^4}\right]\sin 2(\theta-\theta_r) \tag{A10d}$$

where B is the Skempton's pore pressure coefficient, ν_u is the undrained Poisson's ratio, and $\mathrm{K_n}$ is the modified Bessel function of the second kind of order n.

The constants C_1, C_2, C_3 are given by

$$C_1=-\frac{12\xi R(1-\nu_u)(\nu_u-\nu)}{B(1+\nu_u)(D_2-D_1)} \tag{A11a}$$

$$C_2=\frac{4(1-\nu_u)D_2}{(D_2-D_1)} \tag{A11b}$$

$$C_3=-\frac{\xi R(D_2+D_1)+8(\nu_u-\nu)\mathrm{K}_2(\xi R)}{\xi R(D_2-D_1)} \tag{A11c}$$

in which the constants D_1 and D_2 are given by

$$D_1=2(\nu_u-\nu)\mathrm{K}_1(\xi R) \tag{A12a}$$

$$D_2=\xi R(1-\nu)\mathrm{K}_2(\xi R) \tag{A12b}$$

References

[1] Biot, M. A., 1941, "General Theory of Three-Dimensional Consolidation," J. Appl. Phys., **12**, pp. 155–164.

[2] Biot, M. A., 1955, "Theory of Elasticity and Consolidation of a Porous Anisotropic Solid," J. Appl. Phys., **26**, pp. 182–185.

[3] Bear, J., and Corapcioglu, M. Y., 1981, "A Mathematical Model for Consolidation in a Thermoelastic Aquifer Due to Hot Water Injection or Pumping," Water Resour. Res., **17**(3), pp. 723–736.

[4] Kurashige, M., 1989, "A Thermoelastic Theory of Fluid-Filled Porous Materials," Int. J. Solids Struct., **25**(9), pp. 1039–1052.

[5] Coussy, O., 1989, "A General Theory of Thermoporoelastoplasticity for Saturated Porous Materials," Transp. Porous Media, **4**, pp. 281–293.

[6] Coussy, O., 1995, *Mechanics of Porous Continua*, Wiley, New York.

[7] Katsube, N., 1988, "The Anisotropic Thermomechanical Constitutive Theory for Fluid-Filled Porous Materials With Solid/Fluid Outer Boundaries," Int. J. Solids Struct., **24**(4), pp. 375–380.

[8] Utsugida, Y., 1985, "Coupled Analysis of Flow and Heat Around a High-Level Nuclear Waste Repository," in Proc. 5th Int. Conf. Numerical Methods in Geomechanics, Nagoya, Balkema, Rotterdam, pp. 711–716.

[9] Brownell, Jr., D. H., Garg, S. K., and Pritchett, J. W., 1977, "Governing Equations for Geothermal Reservoirs," Water Resour. Res., **13**, pp. 929–934.

[10] Rice, J. R., and Cleary, M. P., 1976, "Some Basic Stress Diffusion Solutions for Fluid-Saturated Elastic Porous Media With Compressible Constituents," Rev. Geophys. Space Phys., **14**(4), pp. 227–241.

[11] Thompson, M., and Willis, J. R., 1991, "A Reformulation of the Equations of Anisotropic Poroelasticity," ASME J. Appl. Mech., **58**, pp. 612–616.

[12] Wang, H., 2000, *Theory of Linear Poroelasticity With Applications to Geomechanics and Hydrogeology*, Princeton University Press, Princeton.

[13] Booker, J. R., and Savvidou, C., 1984, "Consolidation Around a Spherical Heat Source," Int. J. Solids Struct., **20**, pp. 1079–1090.

[14] Booker, J. R., and Savvidou, C., 1985, "Consolidation Around a Point Heat Source," Int. J. Numer. Analyt. Meth. Geomech., **9**, pp. 173–184.

[15] McTigue, D. F., 1986, "Thermoelastic Response of Fluid-Saturated Porous Rock," J. Geophys. Res., **91**(B9), pp. 9533–9542.

[16] McTigue, D. F., 1990, "Flow to a Heated Borehole in Porous, Thermoelastic Rock: Analysis," Water Resour. Res., **26**(8), pp. 1763–1774.

[17] Kurashige, M., 1992, ''Thermal Stresses of a Fluid-Saturated Poroelastic Hollow Cylinder,'' JSME Int. J., **35**(4), pp. 386–391.
[18] Kodashima, T., and Kurashige, M., 1996, ''Thermal Stresses in a Fluid-Saturated Poroelastic Hollow Sphere,'' J. Therm. Stresses, **19**, pp. 139–151.
[19] Cheng, A. H.-D., 1998, ''Material Coefficients of Anisotropic Poroelasticity,'' Int. J. Rock Mech. Min. Sci., **34**, pp. 183–193.
[20] Abousleiman, Y., and Cui, L., 2000, ''The Theory of Anisotropic Poroelasticity With Applications,'' *Modeling and Applications in Geomechanics*, edited by M. Zaman, J. Booker, and G. Gioda, Wiley, New York.
[21] Abousleiman, Y., Cheng, A. H.-D., Cui, L., Detournay, E., and Roegiers, J.-C., 1996, ''Mandel's Problem Revisited,'' Geotechnique, **46**(2), pp. 187–195.
[22] Abousleiman, Y., and Cui, L., 1998, ''Poroelastic Solutions in Transversely Isotropic Media for Wellbore and Cylinder,'' Int. J. Solids Struct., **35**(34/35), pp. 4905–4929.
[23] Li, X., 1992, ''A Generalized Theory of Thermoelasticity for an Anisotropic Medium,'' Int. J. Eng. Sci., **30**(5), pp. 571–577.
[24] Sharma, J. N., and Kumar, V., 1996, ''On the Axisymmetric Problems of Generalized Anisotropic Thermoelasticity,'' J. Therm. Stresses, **19**, pp. 781–794.
[25] Sharma, J. N., and Kumar, V., 1997, ''Plane Strain Problems of Transverse Isotropic Thermoelastic Media,'' J. Therm. Stresses, **20**, pp. 463–476.
[26] Nowacki, W., 1962, *Thermoelasticity*, Addison-Wesley, Reading, MA.
[27] Nowinski, J. L., 1978, *Theory of Thermoelasticity With Applications*, Sijthoff & Noordhoff, Groningen.
[28] Ekbote, S., Abousleiman, Y., and Zaman, M. M., 2000, ''Porothermoelastic Solution for an Inclined Borehole in Transversely Isotropic Porous Media,'' Fourth North American Rock Mechanics Symposium. Seattle, WA, Sept. 5–10.
[29] Ekbote, S., 2002, ''Poromechanics Wellbore Stability: Theory and Applications,'' Ph.D. dissertation, The University of Oklahoma.
[30] Abousleiman, Y., and Ekbote, S., 1999, ''Porothermoelasticity in Transversely Isotropic Porous Materials,'' The IUTAM Symposium on Theoretical and Numerical Methods in Continuum Mechanics of Porous Materials. Stuttgart, Germany, Sept. 5–10, pp. 145–152.
[31] Bird, R. B., Stewart, W. E., and Lightfoot, E. N., 1960, *Transport Phenomena*, Wiley, New York.
[32] Cui, L., Cheng, A. H.-D., and Abousleiman, Y., 1997, ''Poroelastic Solution of an Inclined Borehole,'' ASME J. Appl. Mech., **64**, pp. 32–38.
[33] Cheng, A. H.-D., 1997, ''On Generalized Plane Strain Poroelasticity,'' Int. J. Rock Mech. Min. Sci., **35**, pp. 199–205.
[34] Li, X., Cui, L., and Roegiers, J.-C., 1998, ''Thermoporoelastic Modeling of Wellbore Stability in Non-Hydrostatic Stress Field,'' Int. J. Rock Mech. Min. Sci., **34**(3/4), pp. 829–835.
[35] Nair, R., Abousleiman, Y., and Zaman, M. M., 2002, ''A Finite Element Porothermoelastic Model for Dual-Porosity Media,'' Int. J. Numer. Analyt. Meth. Geomech., **28**(9), pp. 875–898.
[36] Carslaw, H. S., and Jaegar, J. C., 1959, *Conduction of Heat in Solids*, Oxford University Press, New York.
[37] Stehfest, H., 1970, ''Numerical Inversion of Laplace Transforms,'' Commun. ACM, **13**, pp. 47–49; **13**, p. 624.